Development of a Wave-Powered Desalination Device: Numerical Modelling

Conference Paper · August 2017

CITATIONS
0

READS
17

5 authors, including:

Manuel Gerardo Verduzco-Zapata
Universidad de Colima
9 PUBLICATIONS **5** CITATIONS
SEE PROFILE

Francisco J Ocampo Torres
Ensenada Center for Scientific Research and …
67 PUBLICATIONS **736** CITATIONS
SEE PROFILE

Aramis Olivos
Universidad de Colima
51 PUBLICATIONS **111** CITATIONS
SEE PROFILE

Development of a Wave-Powered Desalination Device: Numerical Modelling

Manuel G. Verduzco-Zapata[#1], Francisco J. Ocampo-Torres[#2], Chris Matthews[#3], Aramis Olivos-Ortiz[#1], Diego E. Galván-Pozos[#2]

[#1]*Facultad de Ciencias Marinas, Universidad de Colima,*
Carretera Manzanillo-Barra de Navidad km 19.5 Colonia El Naranjo. C.P. 28868, Manzanillo, Colima, México.
manuel_verduzco@ucol.mx
[#2]*Departamento de Oceanografía Física, Centro de Investigación Científica y de Educación Superior de Ensenada,*
Carretera Ensenada-Tijuana 3918, Ensenada, Baja California, México.
ocampo@cicese.mx
[#3]*SAROS Department, EcoH2O Innovation,*
Charlotte Office, 3120 Latrobe Dr. Suite 270 Charlotte, NC 28211.
cmatthews@sarosdesalination.com

***Abstract*— The lack of fresh water is an increasing worldwide problem caused by the over exploitation and pollution of aquifers and water reserves by anthropogenic activities. In coastal regions, desalination can be used to turn seawater into a new source of fresh water. The aim of this paper is to describe the first stages of development of a Wave Energy Converter which instead of generating electricity desalinates water for human use. This prototype consists of two main subsystems, a wave-powered high-pressure pump and a reverse osmosis system. Through numerical modelling, three different buoys were tested under regular wave conditions in order to evaluate the differences in power transfer from each passing wave into the motion of the buoy. The three buoys had a similar total displacement, meaning their overall ability to provide a force on the system is comparable, but feature different height to diameter ratios. These differing ratios have an effect on the response of the buoy, and subsequently the buoy's efficiency to transforming wave energy into hydraulic energy. Results suggest that the low aspect ratio buoy provides the required force to induce the necessary pressure to make the desalination system to work. This low aspect ratio is preferred as the buoy tended to have minor acceleration jumps, which may reduce the stresses on the connectors and materials of the WEC and the anchor system. These results obtained under controlled conditions will help in the further design of the prototype in order to improve its reliability, survivability, scale as well to reduce its maintenance costs and environmental impact.**

***Keywords*— Desalination system; inverse osmosis; wave energy converter; wave-structure interaction; Flow-3D model.**

I. Introduction

In general, governments around the world are facing a great challenge to secure the fresh water supply in a regular day to day basis and the problem is only getting worse due to the rapidly growing overpopulation and the overexploitation and pollution of water reserves mainly by industrial and housing activities. There is not an easy workaround for this challenge, and the efforts have been focused on finding new deep underground aquifers stressing even more the natural balance of this resource, with evidence of an increasing risk of salty water intrusion in coastal areas as a result of lowering the water table [1]. The contamination and shortage of water supply, coupled with extreme poverty and lack of hygiene, provokes the proliferation of infectious diseases that can affect the population, especially in isolated communities with almost null potable water network. Coastal regions often turn to desalination to access seawater. Desalination, however, requires a large amount of energy. Reverse osmosis (RO) is rapidly gaining popularity due to the continuously decreasing price of the membranes employed in the process [2] and relatively low energy requirements. Nevertheless, the cost of fresh water produced from desalination systems using a conventional source of energy (fossil fuels) ranges between 1 euro m^{-3} and 3.14 euro m^{-3}, with the drawback of increasing the ecological footprint. As an alternative, there are options of using renewable energies as wind, solar and ocean surface waves which may provide the require amount of energy (or the pressure) necessary to force the water flow through the RO membranes. The latter are suitable for desalination as both, the energy and the water are available. For this purpose, the Wave Energy Converters (WEC) must be designed to handle the rigors and the unpredictability of the marine environment. According to their horizontal extension and orientation the WECs can be classified as line or point absorbers [3]. The first one has extensions comparable to the incoming wavelength, and are subdivided in attenuators or terminators (if they are aligned parallel or normal to the direction of wave propagation, respectively). On the other hand, the point absorbers have a small extension compared to the wavelength.

Focusing on the point absorbers, they consist of a buoyant body which uses the vertical motion of each wave and the available buoyant force to produce work, hence they can capture energy from waves traveling in any direction. An advantage over other technologies is that these devices can be deployed both near and off-shore, can be easily designed with minimal submerged mechanical parts, and are relatively easy to model. The dynamics of a point absorber are very similar to

a simple spring-mass-damper with the Power Take-Off (PTO) relying simply on the damped motion of the buoy relative to some fixed point or structure. Many point absorbers, including the one presented in this paper, are designed so to be robust and simple to install, although there are more complex and substantial designs which rely on large off-shore platforms.

Research on point absorbers has produced a variety of developmental insights over the years. According to [3] and [4], the first reported wave-powered desalination system was the DELBUOY [6] which consisted on a single buoy anchored to the seabed using piston pumps, which with every passing wave pressurizes the seawater enough to go through the membranes. Another device is the Mc-Cabe Wave Pump [7] which consists of three rectangular steel pontoons aligned so that their longitudinal direction heads into the incoming waves. The three parts of the pontoon, which are hinged together across their narrowest width, move relative to each other in the waves. Energy is extracted from the rotation about the hinge points by linear hydraulic pumps, pumping the seawater into a RO desalinator. In the Wave-jet prototype [4], the incoming waves are guided over a wave amplifier to be elevated above the sea level in a reservoir. Then, for the purpose of desalination, it is intended to supply this seawater to a pressure intensifier device, supplying a smaller quantity of seawater at sufficient pressure to run a reverse osmosis unit.

The CETO [8] is a fully-submerged point absorber device which produces high-pressure water using the waves motion. It is composed by a buoy submerged few meters below the water surface. The wave action moves the buoy and the energy captured is transferred to a pump. Through delivering high-pressure water on shore, fresh-water can be produced using standard reverse osmosis desalination technology. Another type of desalination device is the OWC Indian plant [9], which harvest wave energy using a semi-submerged chamber and an air turbine. Due to wave actions, the air inside the chamber goes up and down, then a turbine extracts this kinetic energy from the air column and send it to a variable speed alternator to run a desalination plant.

All the devices mentioned above have the general goal of producing enough hydraulic energy to carry out the desalination process. Their efficiency will depend mostly on the dimensions of the buoys, the mooring design and the sea state of the deployment site. [10] studied the possible implementation of a latching control [11,12] on the PTO of a buoy in order to have the velocity and the force reaching their maxima at the same time with the excitation force, with a resulting amplification of the WEC motion. Further developments found that point absorber effectiveness is impacted by buoy ratio, and that it is necessary to control the artificial damping in order to obtain good power capture ratio in different wave climates [13]. The main challenge of implementing these concepts is to introduce optimal algorithms in real life scenarios to control the latching and/or the damping forces in the PTO. This kind of technology is still under development and more research needs to be done to be able to incorporate new components to the pump systems, as a latching control and energy recovery devices (units that allow the use of the remaining kinetic energy from the brine outflow to enhance the required water input).

The aim of this paper is to describe the first stages of development of a point-absorber Wave Energy Converter (WEC) coupled to a desalination system, to directly pump water using only the wave motion. In the next section a brief description of the WEC is presented. In section III and IV the numerical model used in the experiments is described and the results are shown, respectively. Finally, some conclusions are made in section V.

II. WAVE ENERGY CONVERTER

A. *WEC description*

The WEC (Fig. 1) consists of two main subsystems, a wave-powered high-pressure pump, and a reverse osmosis system. The wave-powered pump is a point-absorber type wave energy converter. Most point absorbers suffer from two key challenges: an inability to easily adjust to tidal changes and variations in wave amplitude, and an inability to efficiently resist the motion of the buoy to produce work. This device presents a solution to both of these issues through a patent pending mechanism which eliminates the need for inefficient and cumbersome heave-plates, and still allows for a large range of wave conditions to be used with a taut-line mooring. With each passing wave, line is pulled from the buoy with enough force to drive pumps. These pumps provide the pressure and flow for the reverse osmosis process. After the crest of the wave has passed, the mechanism maintains enough tension in the mooring to restore the buoy to its original position. The reverse osmosis system and pump are comprised of standard, commercially available components. The water is drawn in from the ocean and is forced through sediment filters which produce clean seawater. The water then enters positive displacement piston pumps which pressurize the water to 4.8-6.2 MPa and circulate the water through a reverse osmosis membrane, enhanced by an energy recovery system used to reduce the total amount of energy required in the process. An illustrative diagram of the WEC setup is shown in Fig. 2.

The influence of several variables on the efficiency of the WEC needs to be fully understand prior the further development of the device. Particularly there is a need to test: a) buoys with different sizes and their response to different wave conditions (perhaps the largest disadvantage of point absorbers is that an individual buoy typically has a small area, reducing the overall energy that the device can capture); and b) the overall configuration of the restoring mechanism that is in charge of maintaining the tension in the mooring line. Hence, three different buoy's sizes are proposed, each with a different

aspect ratio defined as the ratio between the buoy's height and its diameter: low (0.35/2), medium (0.50/1.65) and high (0.80/1.30). The dimensions are shown in Fig. 3. Based on previous work done by EcoH2O Innovations, it is proposed that the restoring mechanism has an equivalent spring coefficient k_s of 2.995 N/m, and the calculated force to induced the required pressures is 1.65 kN, which will only be present when the buoy has positive displacements, that is when the mooring line is stretched.

Fig. 1. WEC prototype for desalination purposes (courtesy of EcoH2OInnovation).

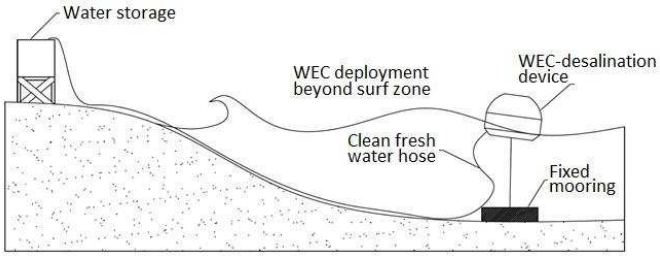

Fig. 2 Diagram of the overall WEC-desalination system (courtesy of EcoH2OInnovation).

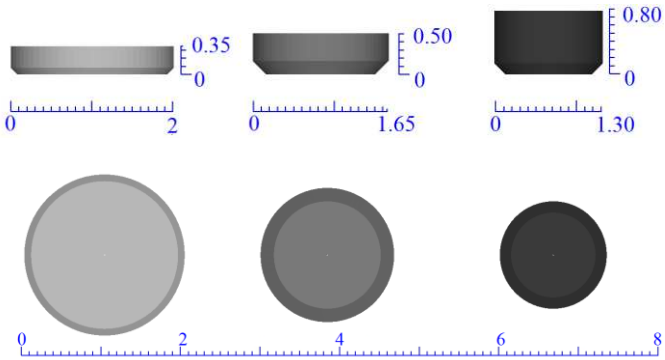

Fig. 3 From top to bottom: (a) lateral view of the three buoys; (b) view from below. Units in meters.

III. NUMERICAL MODEL

A. *Equations*

The FLOW-3D model (F3D) version 11.2.2.01 is a RANS model that solves the continuity equation (Eq. 1) and the three dimensional equations of motion (Eq. 2-4) by finite difference schemes, using a staggered grid with variable rectangular cells sizes in a Cartesian coordinate system. The free surface is solved with the Volume of Fluid technique (VOF) (Eq. 5) [14], which tracks the time-space evolution of the water surface through the computational grid and allows to apply boundary conditions at the surface. The terms in Eqs. 1-5 are defined in Table I, and most of them are evaluated with explicit methods using the available values in every time level requiring a small time step Δt, which can be set constant or dynamically computed to fulfil the Courant condition for computational stability.

$$\frac{\partial u A_x}{\partial x} + \frac{\partial v A_y}{\partial y} + \frac{\partial w A_z}{\partial z} = S_p \tag{1}$$

$$\frac{\partial u}{\partial t} + \frac{1}{V_F}\left\{uA_x\frac{\partial u}{\partial x} + vA_y\frac{\partial u}{\partial y} + wA_z\frac{\partial u}{\partial z}\right\} = -\frac{1}{\rho}\frac{\partial p}{\partial x} + G_x + f_x - b_x + S_u \tag{2}$$

$$\frac{\partial v}{\partial t} + \frac{1}{V_F}\left\{uA_x\frac{\partial v}{\partial x} + vA_y\frac{\partial v}{\partial y} + wA_z\frac{\partial v}{\partial z}\right\} = -\frac{1}{\rho}\left(\frac{\partial p}{\partial y}\right) + G_y + f_y - b_y + S_v \tag{3}$$

$$\frac{\partial w}{\partial t} + \frac{1}{V_F}\left\{uA_x\frac{\partial w}{\partial x} + vA_y\frac{\partial w}{\partial y} + wA_z\frac{\partial w}{\partial z}\right\} = -\frac{1}{\rho}\frac{\partial p}{\partial z} + G_z + f_z - b_z + S_w \tag{4}$$

$$\frac{\partial F}{\partial t} + \frac{1}{V_F}\left[\frac{\partial}{\partial x}\left(FA_x u\right) + \frac{\partial}{\partial y}\left(FA_y v\right) + \frac{\partial}{\partial z}\left(FA_z w\right)\right] = S_F \tag{5}$$

TABLE I
TERMS DEFINITIONS OF EQUATIONS 1-5

Term	Definition
u, v, w	Velocities components in x, y and z direction.
A_x, A_y, A_z	Fractional area opened to flow in each direction.
V_F, F	Fractional volume open to flow and filled volume, respectively.
ρ, p:	Fluid density and pressure, respectively.
b_x, b_y, b_z	Flow losses in porous media in each direction.
G_x, G_y, G_z	Body accelerations in x, y and z directions, respectively.
f_x, f_y, f_z	Viscous accelerations.
S_p, S_u, S_v, S_w, S_F.	Energy input functions with non-zero values only at the inlet boundary and/or near obstacles.

The WEC was implemented blocking partial or totally some specific cells using the Fractional Area/Volume Obstacle Representation (FAVOR) method [15], which defines the fractional areas and volumes of the partially blocked cells. It also flags (using the variable V_F) the cells completely occupied by an obstacle (Fig. 4).

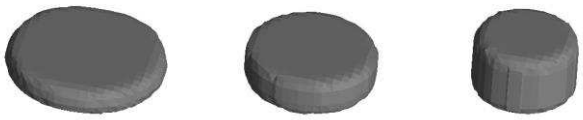

Fig. 4. From left to right: Perspective view of the low, medium and high aspect ratio buoys, respectively, using the FAVOR method within FLOW-3D.

The coupled water-buoy movement is estimated using the General Moving Objects (GMO) model [12] using an implicit method to enhance the numerical stability. This method allows the modelling of body motions in its six degrees of freedom. The buoy system with its origin at its mass centre (G_M) is set up with its coordinate axes parallel to those of the general space system at time t=0. Velocity of any point P on the body is equal to the velocity of the origin G_M plus the velocity due to rotation about G_M (Eq. 6):

$$\bar{V}_p = \bar{V}_G + \bar{\omega} \times \bar{r}_{P/G_M} \tag{6}$$

where $\mathbf{V_P}$, $\mathbf{V_{GM}}$, $\boldsymbol{\omega}$ and $\mathbf{r_{P/GM}}$ are the velocity at P and G_M, the angular velocity, and the distance vector from G_M to P, respectively. The motion is divided into a translational (Eq. 7) and a rotational motion (Eq. 8):

$$\bar{F}_T = m \frac{d\bar{V}_{G_M}}{dt} \tag{7}$$

$$\bar{T}_G = [J] \cdot \frac{d\omega}{dt} + \omega \times \left([J] \cdot \omega \right) \tag{8}$$

where $\mathbf{F_T}$ is the total force, m is the rigid body mass, $\mathbf{T_G}$ is the total torque about G_M, and [J] is the moment of inertia tensor in the body system. At each time step, the locations and orientations of the buoy are tracked and the area and volume fractions are updated by resolving the equations of rigid body motion, considering the effects of hydraulic and gravitational forces [17].

On the other hand, the Renormalized-Group (RNG) model [18] was used to calculate the turbulence associated with the flow-structure interaction, where the influence of the buoyancy forces and the fractional areas/volumes of the FAVOR method are taken into account. The maximum turbulent mixing length used in the RNG model was chosen to be dynamically computed as a function of time and location during simulation, so the calculated turbulent viscosity does not become excessively large. Full details of the mathematical model of the methods described above are given in [19].

B. Numerical wave flume setup

The numerical wave flume (Fig. 5) has a constant depth *h* of 10 meters and it is divided in three mesh blocks. The block I is 70 m long, and it has a uniform mesh with a cell size of 0.10 m with a total of 14,560,000 (700 x 160 x 130) cells. The cell size was chosen to have seven cells per wave height, enough for computing the incoming waves since the FAVOR method does not require a large number of cells to partially block the cells efficiently at the free surface by means of the variables A, V_F and F (the actual recommendation is to use at least four cells per wave height, being six to eight an ideal number [20]). Although a smaller mesh may give more accurate results regarding the buoy movement, the resolution is comparable to other point absorbers studies [21] and it is high enough to obtain reliable results at this initial stage of the WEC development that will serve as a base to design the next tests with higher resolution. Block II and III are 50 and 100 m long, respectively, and conform the dissipation zone. Block II has a coarse mesh of 0.2 m and a total of 1,300,000 (250 x 80 x 65) cells. Finally, Block III has the coarser mesh with a resolution of 0.30 m, with a total of 758,907 (333 x 53 x 43) cells. These coarse meshes will help to diffuse the wave energy numerically. The height and wide of the flume were constant in the three blocks (13 and 16 m, respectively), wide enough to minimize the lateral wall reflections by the radiated waves from the buoy. The initial still water elevation was set at z=0.

The wave boundary was defined at the inlet of block I, while at the outlet boundary of block III a Sommerfeld radiation condition were used to minimize undesired spurious reflections from the open boundary. As the radiation condition alone will not completely eliminate the reflection from the open boundary, a numerical sponge with a length of 150 meters was imposed at block II and III. At the flume bottom and its sides, as well as at solid boundaries, no-slip and impenetrability conditions were applied.

In order to minimize the storage and computational time, top cells were removed from regions where the waves would not reach in the entire simulation. This was done by setting two "domain removing" components as shown in Fig. 5.

Along the channel two sensors were placed to detect the water surface elevation, and one more attached to the WEC to measure its displacement and velocity. Sensor 1 was located at 35 m from the wave source (inlet boundary at the left of the flume) while sensor 2 was at +15 meters after the WEC. Sensor 3 was placed attached to the buoy's mass centre G_M. The time step (Δt) was automatically set so the Courant stability condition was always achieved during the experiment.

The inlet boundary was forced with second order Stokes waves with a wave height H = 0.75 m and a wave period T = 3.90 s, as shown in Table I. The wave steepness is 0.03 in all tests. These parameters were selected in order to represent low energy sea states, with relatively small wavelengths and wave heights. In further experiments it will be required to extend the experimental design to include more wave scenarios including irregular waves (out of the scope of this paper).

The tests were carried on a server with 1 processor Intel Xeon E5-2690 v4 @2.6 GHz with 14 cores, 64 GB of RAM and 1 TB of solid hard drive.

TABLE II
EXPERIMENTAL MATRIX

Buoy's aspect ratio (d/D)	**H (m)**	***k_r* (*N/m*)**	***k_s* (*N/m*)**	**T (s)**	**h (m)**
-	0.75	-	-	3.90	10
Low (0.35/2)	0.75	4,400	2.995	3.90	10
Medium (0.50/1.65)	0.75	4,400	2.995	3.90	10
High (0.80/1.30)	0.75	4,400	2.995	3.90	10

where d and D are the height and diameter of the buoy, respectively; H and T are the wave height and period, respectively; h is the water depth; and k_r and k_s are the rope and spring coefficient, respectively.

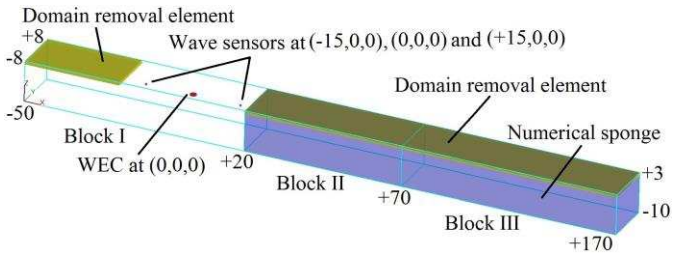

Fig. 5 Numerical wave tank configuration with a length of 220m conformed by three mesh blocks each with 10m depth and 16m wide. Block II and III are used as damping zones.

C. WEC implementation

The WEC buoy has a density of 163 kgm^{-3}, while the fluid was set to 1000 kgm^{-3}. Three different aspect ratios (low, medium and high) of the buoy were tested in order to evaluate its efficiency and overall hydrodynamic performance, and to find the best setup for the pumping system, giving a specific sea state associated with places with low wave energy conditions. As mention above, the FAVOR method was employed to represent the moving devices by blocking the corresponding cells (Fig. 4).

The restoring mechanism employed for maintaining the tension in the mooring line was simulated using a spring with a free length of 10 m with a maximum compression and extension length of ±1 m and a spring coefficient k_s of 2.995 N/m. Then the spring exerts the forces corresponding to the restoring force of the line which attaches the buoy to the load anchor. On the other hand, the PTO was simulated using a massless elastic rope with the same dimensions of the spring, with a spring coefficient k_r of 4.40 *k*N/m. The rope exerts a force only when it is stretched, representing the dampening due to the pumping system.

Both, the spring and the rope follows a straight line between the anchor point and the moving buoy, representing well the PTO and the spooled-line system. A further refining for incoming studies will be to substitute the rope with the actual PTO system, which will require an even higher resolution mesh.

A simplified loading diagram is shown in Fig. 6. The total force (F) on the device is the sum of the restoring force (2.995 N/m times the spring extension, Z_s) plus the force exerted by the pumping system (0 to 1.65 kN when the rope extension Z_r is greater than zero). The pump is designed for a maximum force load of 1.65 *k*N.

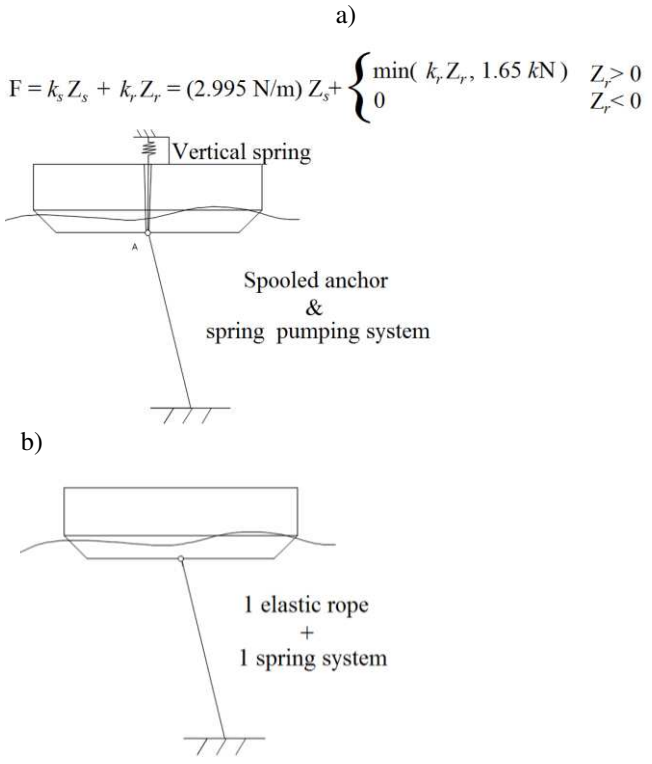

Fig. 6 WEC's diagram: a) actual loading; b) simplified loading on the buoy.

IV. Results and Discussions

D. Model validation: surface water elevation

The first experiment was set up without the WEC to validate the quality of the generated waves. As expected, the first periods showed uneven wave heights due to an increasing wave ramp. In order to have a constant wave height, the first eight periods were removed to eliminate the wave irregularity from the records. The final time series of the water elevation is shown in Fig. 7. A zero-crossing method was employed to calculate the wave parameters, resulting in a wave height of 0.749 m and a period of 3.95 s. The results showed a good agreement with the targeted values of Table I, with an error lower than 0.10% and 1.3% for the wave height and period, respectively.

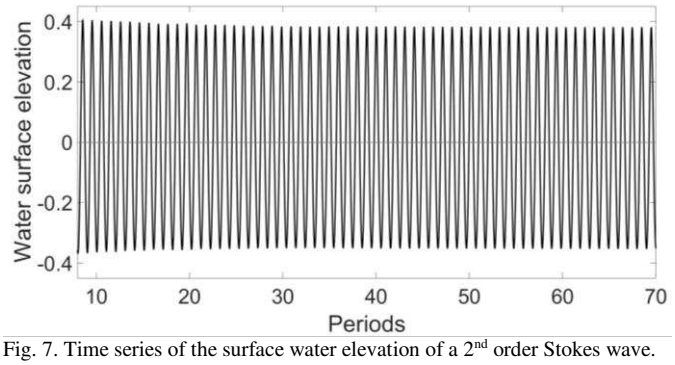

Fig. 7. Time series of the surface water elevation of a 2nd order Stokes wave.

E. Buoys displacements, velocities and accelerations

The displacements, velocities and accelerations of the buoy are shown in Figs. 8 and 9. For ease of visualization, only the data of a six period window was plotted. Fig. 8 shows the surge, heave and sway motions of the three different buoys used in the WEC system, each with different aspect ratio (low, medium and high). The tree buoys showed similar responses to wave motion in heave and sway displacements, although the surge motion was highest for the high aspect buoy, followed by the medium and then the low aspect ratio buoy. Vertical velocities are very close to each other in each case except at wave crests that in turn makes the low aspect buoy acceleration quite different compared with the other, being significantly lower in this case (Fig. 9). The maximum accelerations occur in the medium and high cases, due to the rapidly velocities changes that occur when these buoys reach the wave crests, while the low buoy is more stable. In the rest of the wave phases, far from the crests, the accelerations are similar in every case.

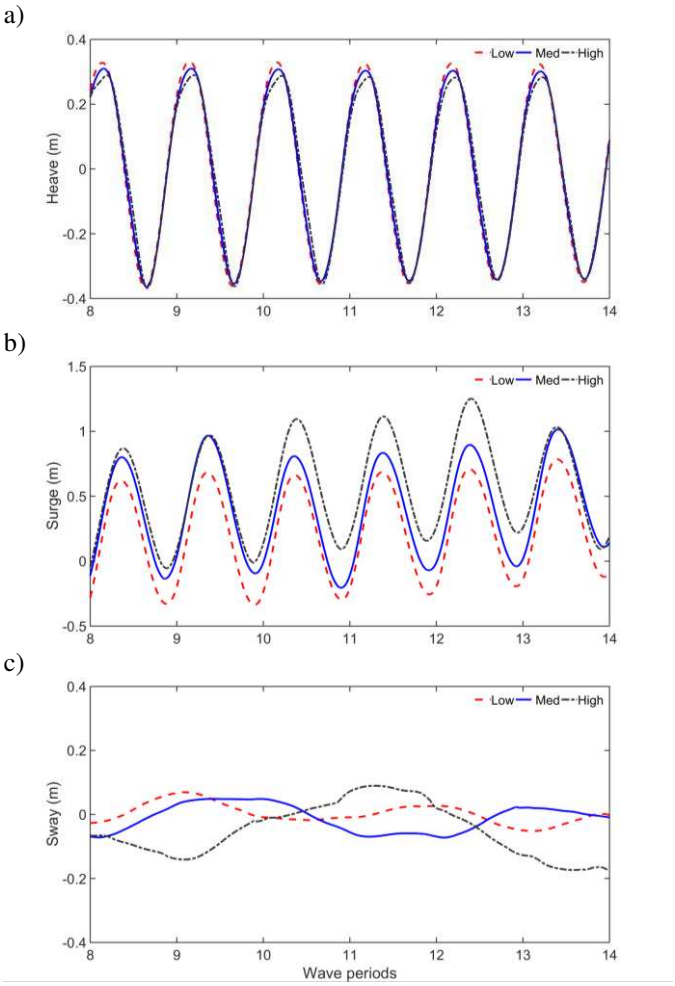

Fig. 8. Linear displacements of the low, medium and high aspect ratio buoys: (a) z-direction (heave), (b) x-direction (surge), and (c) y-direction (sway).

F. WEC efficiency

The WEC efficiency can be initially estimated by analysing the forces applied on the restoring force line (spring) and the pump line (rope). With every wave crest, the buoy pulled the rope and the spring by the same amount in the positive direction (line elongation), with a negative (restoring) force along the line of action of the spring. The results are plotted in Figs. 10, 11 and 12, where it can be seen that the buoy with lowest aspect ratio showed a slightly best performance compared with the other configurations as the rope tension, representing the required force for water pumping, is closest to the maximum design value of 1.65 kN. In addition, the lowest aspect ratio buoy tended to have minor acceleration jumps, which may reduce the stresses on its connectors and materials (Fig. 9). The spring mechanism had smooth positive and negative displacements with the passes of every wave crest. The exerted forces on the mechanism (Fig. 11) as well as the kinetic energy (Fig. 12) were also similar in the three cases. No excessive forces were present during the tests. Nevertheless, it is expected that with higher wave

heights the pump's estimated maximum required force of 1.65kN will be exceeded, then the buoy needs to include specially designed escape valves to avoid excessive pressures at the hydraulic system of the WEC or on the membranes. Moreover, it will be necessary to design an adequate damping system to avoid an abrupt stop of the WEC's motion, otherwise excessive forces may appear damaging the anchor system.

The results are promising and future designs may include the use of the Stewart Gough platform concept [22], which may improve the overall efficiency of the WEC [23]. There is a necessity of incorporating an Energy Recovery Device (ERD) and the RO membranes effects into the numerical simulations in order to better represent the physics of the system, and then be able to find the best configuration to induce a fairly constant flow in order to make the process as efficient as possible.

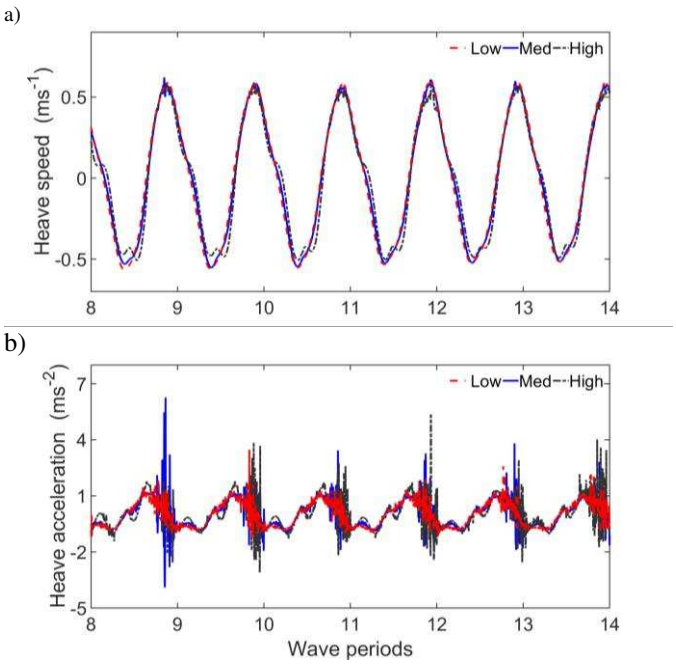

Fig. 9. (a) Vertical velocities and (b) vertical acceleration of the low, medium and high aspect ratio buoys.

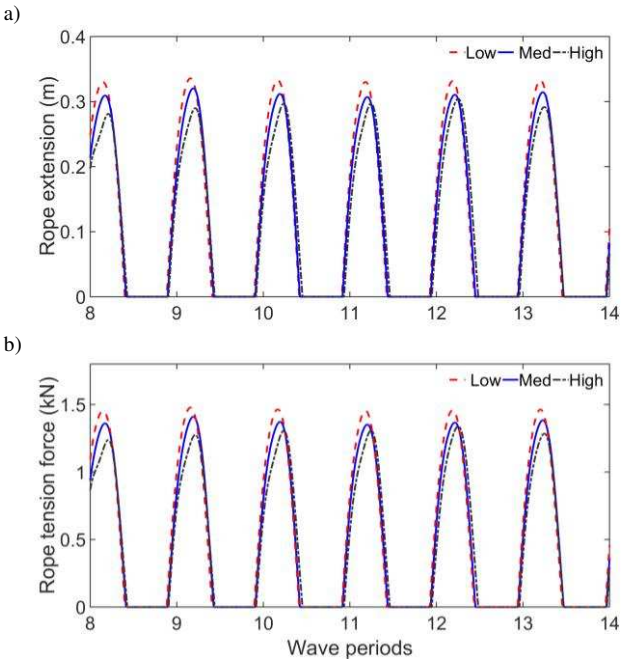

Fig. 10. (a) Rope extension of the three buoys (metres); and (b) rope tension force (kN).

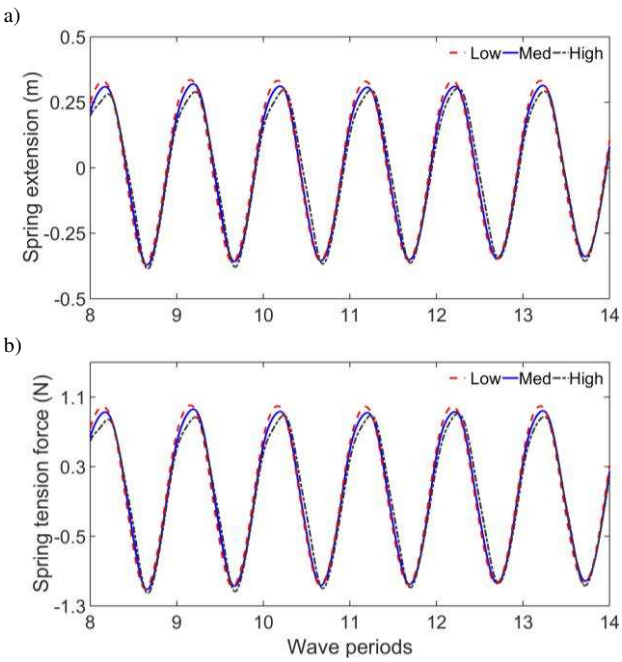

Fig. 11. (a) spring force (N); and (b) spring extension (metres).

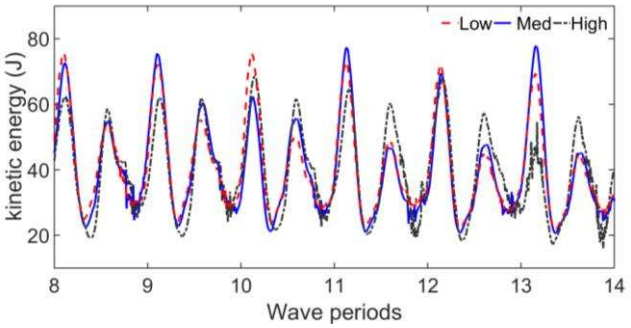

Fig. 12. Buoy kinetic energy of the low, medium and high aspect ratio buoys.

V. Conclusions

The Wave Energy Converter for desalination purposes described in this document is based on the SAROS system and its performance under a train of second order Stokes waves was studied. Results suggest that the pumping mechanism works slightly better with a low aspect ratio buoy, which provides the required force to induce the necessary pressure to make the sea water flow through the inverse osmosis membranes.

It is expected that with higher wave heights the pump's estimated maximum required force will be exceeded, then a specially design mechanism to avoid excessive pressures and forces will be required. This mechanism could consist on a) escape valves in the hydraulic system to prevent its failure, and b) a robust damping system to prevent the occurrence of large impulse forces due to an abrupt stop of the WEC. Moreover, the efficiency of the WEC can be maximized with the proposal of a latching control on the PTO of the buoy in order to have the pumping force reaching their maxima at each wave crest, with a resulting amplification of the WEC motion. The design of these elements (valves, damping mechanisms and the latching control system) represent an interesting challenge, as their numerical implementation is not straight forward, and the optimum damping mechanism needs to be found and dynamically changed in order to approximate the natural frequency of the WEC with the mean frequency of the incoming waves.

More numerical tests are needed with more sea states (with both regular and irregular waves) associated to low wave energy conditions (*e.g.* the Mexican Pacific) in order to select a final design of the buoy and the anchor system, and then start the validation with physical experiments in a wave flume and basin. Finally, it is worth mention that in the next steps of the research it would be interesting to modify the WEC configuration using the Stewart Gough platform concept, as it has been demonstrated that under this setup the WEC could drastically improve its efficiency.

Acknowledgment

This work has been developed under the research program of the Wave Group at Colima University (UCOL) and CICESE, supported by CONACYT (project PN-2015-01-674) and CEMIE-O. The authors would like to thank UCOL for the the GEOS1 server support, as well as EcoH2OInnovation for the SAROS data.

References

[1] Barlow P, Reichard E. Saltwater intrusion in coastal regions of North America. Hydrogeology Journal 2010;18:247–60.
[2] Karagiannis I, Soldatos P. Water desalination cost literature: review and assessment. Desalination 2008;223:448–56.
[3] Falnes J. A review of wave-energy extraction. Marine Structures 2007;20:185–201.
[4] Davies P. Wave-powered desalination: resource assessment and review of technology. Desalination 2005;186:97–109.
[5] Gude V, Nirmalakhandan N, Deng S. Renewable and sustainable approaches for desalination. Renewable and Sustainable Energy Reviews 2010;14:2641–54.
[6] Hicks D, Mitcheson G, Pleass C, Salevan J. Delbouy: ocean wave-powered seawater reverse osmosis desalination systems. Desalination 1989;73:81–94.
[7] Brooke J. Wave energy conversion. 1st ed. Hungary: Elsevier Science; 2003.
[8] Karimirad M. Offshore energy structures: for wind power, wave energy and hybrid marine platforms. Switzerland: Springer; 2014.
[9] Sharmila N, Jalihal P, Swamy A, Ravindran M. Wave powered desalination system. Energy 2004;29:1659–72.
[10] Clément A, Babarit A. Discrete control of resonant wave energy devices. Philosopphical Transactions or the Royal Society 2012;370:288–314.
[11] Budal K, Falnes J, Iversen L, Lillebekken P, Oltedal G, Hals T, et al. The Norwefian wave-powered buoy project. Proceedings of the the second International Symposium on Wave Energy Utilization, Trondheim: 1982, p. 323–44.
[12] Falnes J. Principles for capture of energy from ocean waves. Phase control and optimum oscillation. Trondheim, Norway: 1997.
[13] Eriksson M, Isberg J, Leijon M. Hydrodynamic modelling of a direct drive wave energy converter. International Journal of Engineering Science 2005;43:1377–87.
[14] Hirt C, Nichols B. Volume of fluid (VOF) method for the dynamics of free boundaries. Journal of Computational Physics 1981;39:201–25.
[15] Hirt C, Sicilian J. A porosity technique for the definition of obstacles in rectangular cell meshes. 1985.
[16] Wei G. A fixed-mesh method for General Moving Objects (Technical note FSI-05-TN73). 2005.
[17] Wei G. A fixed-mesh method for General Moving Objects in Fluid Flow. Modern Physics Letters 2005;19:1719–22.
[18] Yakhot V, Thangam S, Gatski T, Orszag S, Speziale C. Development of turbulence models for shear flows by a double expansion technique. 1991.
[19] Flow-Science. FLOW-3D user manual 2014:981.
[20] Flow-Science Inc. Waves – Best Practices Part I of modeling the marine environment. Proceedings of the 2012 FLOW-3D World Users Conference, San Francisco, CA.: Flow-Science, Inc.; 2012, p. 1–31.
[21] Bhinder M, Mingham C, Causon D, Rahmati M, Aggidis G, Chaplin R. Numerical and Experimental Study of a Surging Point Absorber Wave Energy Converter. Proceedings of the 8th European Wave and Tidal Energy Conference., Uppsala, Sweeden: 2009, p. 1–6.
[22] Fitcher E. A Stewart Platform-Based Manipulator: General Theory and Practical Construction. The International Journal of Robotics Research 1986;5:157–82.

[23] Verduzco-Zapata, M.; Ocampo-Torres F. Study of a 6 DOF wave energy converter interacting with regular waves using 3D CFD. Proceedings of the 11th European Wave and Tidal Energy Conference, 2015, p. 1–6.